

# Coherent oscillations between two weakly coupled Bose-Einstein Condensates: Josephson effects, $\pi$ -oscillations, and macroscopic quantum self trapping

S. Raghavan<sup>1</sup>, A. Smerzi<sup>2</sup>, S. Fantoni<sup>1,2</sup>, and S. R. Shenoy<sup>1</sup>

1) *International Centre for Theoretical Physics, I-34100, Trieste, Italy*

2) *Istituto Nazionale de Fisica della Materia and International School for Advanced Studies, via*

*Beirut 2/4, I-34014, Trieste, Italy*

(November 26, 2024)

## Abstract

We discuss the coherent atomic oscillations between two weakly coupled Bose-Einstein condensates. The weak link is provided by a laser barrier in a (possibly asymmetric) double-well trap or by Raman coupling between two condensates in different hyperfine levels. The Boson Josephson Junction (BJJ) dynamics is described by the two-mode non-linear Gross-Pitaevskii equation, that is solved analytically in terms of elliptic functions. The BJJ, being a *neutral*, isolated system, allows the investigations of new dynamical regimes for the phase difference across the junction and for the population imbalance, that are not accessible with Superconductor Josephson Junctions (SJJ). These include oscillations with either, or both of the following properties: 1) the time-averaged value of the phase is equal to  $\pi$  ( $\pi$  - *phase* oscillations); 2) the average population imbalance is nonzero, in states with “macroscopic quantum self-trapping” (MQST). The (non-sinusoidal) gener-

alization of the SJJ ‘ac’ and ‘plasma’ oscillations and the Shapiro resonance can also be observed. We predict the collapse of experimental data (corresponding to different trap geometries and total number of condensate atoms) onto a single universal curve, for the inverse period of oscillations.

Analogies with Josephson oscillations between two weakly coupled reservoirs of  $^3\text{He-B}$  and the internal Josephson effect in  $^3\text{He-A}$  are also discussed.

PACS: 03.75.Fi,74.50.+r,05.30.Jp,32.80.Pj

## I. INTRODUCTION

Bose-Einstein condensation, predicted more than 70 years ago [1], was detected in 1995, in a weakly interacting gas of alkali atoms held in magnetic traps [2]. Following the first observations, there have been important experimental developments. A superposition of condensate atoms in different hyperfine levels [3,4] has been created; non-destructive, *in situ*, detection probes have tracked the dynamical evolution of a single condensate [5]. Further, the evolution of the relative phase of two condensates has been measured through interferometry techniques [6]. More recently, experiments that tune the scattering length by several orders of magnitude [7] have opened the definite possibility of creating in the laboratory an ideal condensate of non-interacting atoms.

The precise manipulation of this form of matter is of considerable theoretical interest: besides the study of fundamental aspects of superfluidity from “first principles”, it is possible to address “foundational” problems of quantum mechanics [8]. In fact, the order parameter can be identified with the one-body macroscopic condensate wave function. This obeys a nonlinear Schrödinger equation, known in the literature as the Gross-Pitaevskii equation (GPE) [9]. The GPE has been successfully applied to study kinetic properties of the condensate, like collective mode frequencies of trapped Bose-Einstein condensates (BEC) [10] and the relaxation times of monopolar oscillations [11]. Chaotic behavior in dynamical quantum observables [11,12], and the metastability of quantized vortices has been predicted [13].

The existence of spatial quantum coherence was demonstrated by cutting a single trapped condensate by a far off-resonant laser sheet. Upon switch-off of the confining trap and the laser, the two condensates overlapped, producing interference fringes [14], in analogy with the a double-slit experiment with single electrons.

However, the superfluid nature of BEC can be fully tested only through the existence of superflows. Current experimental efforts are being focused on the creation of a Josephson junction between two condensate bulks [14,15]. In this context, the Josephson junction problem has been studied theoretically in the limit of non-interacting atoms [16], for small

amplitude Josephson oscillations [17,18], including finite temperature (damping) effects [18]. Furthermore, in connection with the quantum measurement problem, decoherence effects and quantum corrections to the semiclassical mean-field dynamics [19,20] have also been studied. Self trapping dynamics in the limit of small number of condensate atoms has been considered [19] in the “quantum” and in the “semiclassical” (mean-field) approximation. We have elsewhere, [21], pointed out that even though the Boson Josephson Junction (BJJ) is a *neutral*-atom system, it can still display the (non-sinusoidal generalization of) typical ‘dc’, ‘ac’ and Shapiro effects occurring in charged Cooper-pair superconducting junctions. Moreover, novel dynamical regimes like macroscopic quantum self trapping (for arbitrarily large condensates) and  $\pi$ -phase oscillations (where the average value of the phase across the junction is equal to  $\pi$ ), have been predicted. In the present paper we present a comprehensive analysis of the effects described in [21], including a discussion of the BJJ equations and their analytic solution, and limits of the approximations underlying the BJJ model, and a comparison with other superconducting and superfluid Josephson junctions.

The description of the GPE dynamics for a Bose condensate in a double-well trap reduces, under certain conditions, to a nonlinear, two-mode equation for the time-dependent amplitudes  $\psi_{1,2}(t) = \sqrt{N_{1,2}(t)}e^{i\theta_{1,2}(t)}$ , where  $N_{1,2}(t)$  and  $\theta_{1,2}(t)$  are the number of atoms and the phases of the condensate in the trap 1,2 respectively. These amplitudes are coupled by a tunneling matrix element between the two traps, with the spatial dependence of the GPE wave function integrated out into constant parameters. The resulting BJJ tunneling equations resemble the (nonlinear generalizations of) Superconductor Josephson Junction (SJJ) equations, with the variables being the relative phase and the fractional population imbalance.

However, there are important physical differences between the isolated double-well BJJ and the SJJ with an external circuit. The SJJ is generally discussed in terms of a rigid pendulum analogy in the resistively shunted junction (RSJ) model, while the BJJ in a double-well trap can only be completely understood in terms of a *non-rigid* pendulum analogy, with a length dependent on the angular momentum. In SJJ the Cooper-pair population

imbalance is identically zero (considering two equal-volume superconducting grains) due to the presence of the external circuit [22], and the dynamical variable is the voltage  $\sim \dot{\phi}$  across a quasiparticle resistive shunt. In the BJJ, the non-rigid pendulum dynamics are associated with *superfluid density* oscillations, of an isolated system. An isolated (without external circuit) superconducting junction allows coherent Cooper-pair oscillations, but only in the small amplitude (plasma) limit [22–24].

A closer analog of the BJJ is provided by the internal Josephson effect in  $^3\text{He-A}$ , where the (rigid) pendulum oscillations describe the rate of change of up and down spin-pair populations, induced by an external variable magnetic field [25–27]. The “ $\pi$  oscillations” between two weakly coupled reservoirs of  $^3\text{He-B}$  [28] could be related to the analogous oscillations occurring in BJJ.

The experimental detection of predicted effects in BJJ could be achieved through temporal modulations of phase-contrast fringes [14], interferometric techniques [6], or other probes of atomic populations [29], using  $\sim$  millisecond temporal oscillations of the integrated signal  $N_1 - N_2$ . The direct detection of the currents instead of densities, perhaps by Doppler interferometry, would be worth exploring.

The plan of the paper is as follows: In Section II, we obtain the BJJ tunneling equations, that, in Section III, are compared with the Josephson equation for other superconductor and superfluid systems. In Section IV we solve the BJJ equations discussing the various dynamical regimes. In Appendix A we outline the derivation of the two-mode BJJ from GPE and discuss the limit of the approximations. The BJJ equations are solved analytically in terms of elliptical functions in Appendix B. In the remainder of the paper Section V, we discuss the asymmetric trap case, clarifying the analogies with the *ac* and Shapiro effect. We summarize our results in Section VI.

## II. BOSON JOSEPHSON JUNCTION: THE NON-LINEAR TWO-MODE APPROXIMATION

The wavefunction  $\Psi(r, t)$  for an interacting BEC in a trap potential  $V_{trap}(r, t)$  at  $T = 0$  satisfies the GPE:

$$i\hbar \frac{\partial \Psi(r, t)}{\partial t} = -\frac{\hbar^2}{2m} \nabla^2 \Psi(r, t) + [V_{trap}(r) + g_0 |\Psi(r, t)|^2] \Psi(r, t), \quad (2.1)$$

with  $g_0 = 4\pi\hbar^2 a/m$ ,  $m$  the atomic mass, and  $a$  the  $s$ -wave scattering length of the atoms [30]. In the following we will consider a double-well trap produced, for example, by a far off-resonant laser barrier that cuts a single trapped condensate into two (possibly asymmetric) parts [14]. However, the results could also apply to the oscillations of the condensate population difference between two hyperfine levels [15].

Since we are interested in the dynamical oscillations of the two weakly linked BEC, we write a (time-dependent) *variational* wave-function as:

$$\Psi(r, t) = \psi_1(t)\Phi_1(r) + \psi_2(t)\Phi_2(r) \quad (2.2)$$

with  $\psi_{1,2}(t) = \sqrt{N_{1,2}} e^{i\theta_{1,2}(t)}$  and a constant total number of atoms  $N_1 + N_2 = |\psi_1|^2 + |\psi_2|^2 = N_T$ . The amplitudes for general occupations  $N_{1,2}(t)$ , and phases  $\theta_{1,2}(t)$  obey the nonlinear two-mode dynamical equations [18–21,31,32],

$$i\hbar \frac{\partial \psi_1}{\partial t} = (E_1^0 + U_1 N_1) \psi_1 - \mathcal{K} \psi_2 \quad (2.3a)$$

$$i\hbar \frac{\partial \psi_2}{\partial t} = (E_2^0 + U_2 N_2) \psi_2 - \mathcal{K} \psi_1, \quad (2.3b)$$

where damping and finite temperature effects are ignored. Here  $E_{1,2}^0$  are the zero-point energies in each well,  $U_{1,2} N_{1,2}$  are proportional to the atomic self-interaction energies, and  $\mathcal{K}$  describes the amplitude of the tunneling between condensates, see Fig. 1. The constant parameters  $E_{1,2}^0, U_{1,2}, \mathcal{K}$  can be written in terms of  $\Phi_{1,2}(r)$  wave-function overlaps. The  $\Phi_{1,2}(r)$ , roughly describing the condensate in each trap, can be expressed in terms of stationary symmetric and antisymmetric eigenstates of GPE, (see Appendix A).

The fractional population imbalance

$$z(t) \equiv (N_1(t) - N_2(t))/N_T \equiv (|\psi_1|^2 - |\psi_2|^2)/N_T \quad (2.4)$$

and relative phase

$$\phi(t) \equiv \theta_2(t) - \theta_1(t) \quad (2.5)$$

obey

$$\dot{z}(t) = -\sqrt{1 - z^2(t)} \sin(\phi(t)), \quad (2.6a)$$

$$\dot{\phi}(t) = \Delta E + \Lambda z(t) + \frac{z(t)}{\sqrt{1 - z^2(t)}} \cos(\phi(t)), \quad (2.6b)$$

where we have rescaled to a dimensionless time,  $t2\mathcal{K}/\hbar \rightarrow t$ , and

$$\Delta E \equiv (E_1^0 - E_2^0)/2\mathcal{K} + (U_1 - U_2)/2\mathcal{K}, \quad (2.7a)$$

$$\Lambda \equiv UN_T/2\mathcal{K}; \quad U \equiv (U_1 + U_2)/2 \quad (2.7b)$$

The dimensionless parameters  $\Lambda$  and  $\Delta E$  determine the dynamic regimes of the BEC atomic tunneling. The total, conserved energy is:

$$H = \frac{\Lambda z^2}{2} + \Delta E z - \sqrt{1 - z^2} \cos \phi. \quad (2.8)$$

suggesting that the equations of motion (2.6) can be written in the Hamiltonian form

$$\dot{z} = -\frac{\partial H}{\partial \phi}; \quad \dot{\phi} = \frac{\partial H}{\partial z}, \quad (2.9)$$

with  $z$  and  $\phi$ , the canonically conjugate variables.

For well defined mean values in relativ population and phase, fluctuations must be small.

### III. THE JOSEPHSON EFFECT IN OTHER SUPERFLUID AND SUPERCONDUCTING SYSTEMS

**The superconducting Josephson Junction (SJJ).** We now consider the SJJ dynamic equations [22–24,33], for comparison with the BJJ tunneling equations of Eq. (2.6).

The SJJ has an external closed circuit that typically includes a current drive  $I_{ext}$ ; the measurable developed voltage across the junction  $V$  is proportional to the rate of change of phase:

$$I_{ext} = C_J \frac{dV}{dt} + I_J \sin \phi + \frac{V}{R} \quad (3.1a)$$

$$\dot{\phi} = \frac{2eV}{\hbar} \quad (3.1b)$$

where  $C_J(I_J)$  is the junction capacitance (critical current) and  $R$  is the effective resistance offered by the quasiparticle junction and the circuit shunt resistor. The  $\sqrt{1-z^2}$  factors of Eq. (2.6) are missing here, since the external circuit suppresses charge imbalances, i.e.  $z(t) \equiv 0$  [22]. The junction charging energy  $E_C \sim C_J^{-1}$ ; superconductor-grain charging energies  $E_{CG}$  ( $\sim$  inverse grain sizes) that are the analogs of interatom interactions  $U$  of the BJJ, are relevant only in mesoscopic systems. Two such small isolated grains [34] can be considered a closer superconducting analog of BJJ. Even in that case, as  $N_T$  is still large, the voltages that appear are  $2eV \sim 2\Delta_{qp}$ , the quasiparticle gap, implying that  $|z| \sim 10^{-9}$ .

Mechanical analogs have been useful in visualizing the SJJ. Equation (3.1) can be written as

$$\ddot{\phi} + \dot{\phi}/RC_J + \omega_J^2 \sin \phi = (I_{ext}/I_J)\omega_J^2 \quad (3.2)$$

in unscaled units, with  $\omega_J = \sqrt{E_C E_J}/\hbar$ , the Josephson plasma frequency. This can be regarded as the equation for a ‘particle’ of ‘mass’  $\sim \omega_J^{-2}$  and ‘position’  $\phi$  moving on a tilted, rigid ‘washboard’ potential  $-\cos \phi - (I_{ext}/I_J)\phi$ , with friction coefficient  $\sim 1/RC_J$ . Alternatively, Eq. (3.1) describes [33] a rigid pendulum of tilt-angle  $\phi$ ; moment of inertia  $\sim \omega_J^{-2}$ ; angular momentum  $V \propto \dot{\phi}$  the angular velocity; damping rate  $(RC_J)^{-1}$  and external torque  $\sim I_{ext}$ .

The Josephson effects in SJJ follow at once from physical considerations:

*Plasma oscillations:* For  $I_{ext} = 0$ , the rigid pendulum can have small, harmonic oscillations in angle  $\phi$  around the vertical. Linearizing Eq. (3.1) produces sinusoidal voltage/current ‘plasma’ oscillations of angular frequency (in unscaled units)



$$\omega \approx \omega_p \equiv 2\pi/\tau_p = \sqrt{E_c E_J}/\hbar, \quad (3.3)$$

independent of initial conditions  $\phi(0), \dot{\phi}(0)$ .

*ac effect:* In the pendulum analogy, the external drive balanced by the damping enforces steady rotatory motion for  $I_{ext}/I_J > 1$ . The phase increases linearly with time,  $\phi(t) \sim 2eVt/\hbar$ , where  $V = I_{ext}R$  is the dc voltage developed, and the current oscillation has angular frequency

$$\omega = \omega_{ac} = \frac{2\pi}{\tau_{ac}} = \frac{2eV}{\hbar}, \quad (3.4)$$

independent of  $\phi(0), \dot{\phi}(0)$ .

*Shapiro resonance effect:* If a small ac component is added to an applied dc voltage,  $\Delta E \rightarrow \Delta E(1 + \delta_0 \cos \omega_0 t)$ ;  $\delta_0 \ll 1$ , then at resonance  $\omega_0 = \omega_{ac}$ , there is a dc tunneling current with a nonzero time average  $\langle \dot{z}(t) \rangle \sim \delta_0 \langle \sin(\omega_{ac} t + \phi(0)) \sin \omega_0 t \rangle \neq 0$ . This Shapiro resonance repeats at higher harmonics  $\omega_{ac} = 2\pi/\tau_{ac} = n\omega_0, n = 1, 2, \dots$ , with characteristic Bessel function coefficients  $J_n(n\delta_0)$  [22,23].

Can the BJJ show the full range of SJJ effects? Not at first sight, since the double-well BEC is a neutral-atom system. However, the ability to tailor traps and the condensate self-interaction compensates for electrical neutrality [21]. Asymmetric positioning of the laser barrier could produce a zero-point energy difference  $\Delta E$ , analogous to an applied voltage, since the effective potential seen by the atoms on the smaller-volume side will have a larger curvature. The interwell difference between the (bulk) nonlinear atomic self-interaction,  $\sim UN_T z$  plays the role of a junction capacitance energy in the dynamics.

In the SJJ,  $E_J$  as well as  $N_{1,2}$  are fixed [22,23]. For the BJJ, the laser-sheet intensity, and hence the coupling  $\mathcal{K}$ , can be varied. Initial states,  $N_1(0) \neq N_2(0)$ , i.e.,  $z(0) \neq 0$ , can be prepared, and the laser barrier then lowered to permit tunneling.

**The internal Josephson effect in  $^3\text{He-A}$ .** A closer analog of the BJJ Eqs. (2.6) is provided by the longitudinal magnetic resonance in  $^3\text{He-A}$  [25], that is generally understood as internal Josephson oscillations between two interpenetrating populations of superfluid

up-down spin-pairs [26]. The weak coupling is provided by the dipole interaction between pairs of up and down spins. The spin dynamics is governed by [27]:

$$\dot{z}(t) = -\sin(\phi(t)), \quad (3.5a)$$

$$\dot{\phi}(t) = \Delta E + \Lambda z(t) \quad (3.5b)$$

where  $z(t)$  is the fractional population imbalance between up and down spin Cooper pairs,  $\Lambda \propto (\chi g_D)^{-1}$  with  $\chi, g_D$  the susceptibility and the dipole coupling respectively, and  $\Delta E \propto (B/\chi g_D)$  with  $B$  the external applied static magnetic field. In [25] experiments have confirmed Eqs. (3.5), showing the transient between the small amplitude and ringing oscillations of the pendulum equations Eqs. (3.5).

**Josephson Oscillations between two weakly linked reservoirs of  $^3\text{He-B}$ .** Quite recently the first direct experimental observation of Josephson oscillations between two weakly linked superfluid systems has been reported [35,36]. The weak link was provided by  $\sim 4000$  small holes in the rigid partition separating two  $^3\text{He-B}$  superfluid reservoirs, with the hole diameter being comparable to the coherence length. A soft membrane created a pressure difference across the weak link, inducing Josephson mass current oscillations. These oscillations obey:

$$I(t) = I_c \sin(\phi(t)), \quad (3.6a)$$

$$\dot{\phi}(t) = -\frac{2m_3}{\hbar\rho} \Delta P \quad (3.6b)$$

with  $2m_3$  the mass of a  $^3\text{He}$  Cooper pair,  $\rho$  the liquid density and  $\Delta P$  the pressure difference across the weak link being proportional to the elastic constant of the membrane. Small and large amplitude oscillations have been observed, as well as the driven running solutions of the phase  $-\infty < \phi < \infty$  [36], corresponding to a self-maintained population across the weak link.

By driving the soft membrane in resonance with the natural Josephson frequency, a new metastable dynamical regime was observed, with the time-averaged value of the phase-difference across the junction equal to  $\pi$ . These metastable ‘ $\pi$ -oscillations’ have amplitudes

and frequencies smaller than the ‘stable’ Josephson oscillations, into which they decay with a life time that increases with decreasing temperature [28]. Analogous  $\pi$ -oscillations with similar properties are described by BJJ (see Section IV). In a different context,  $\pi$ -junctions have been created with high- $T_c$  superconductors, that reflect the symmetry of the  $d$ -wave pairing state [37].

#### IV. THE SYMMETRIC TRAP CASE, $\Delta E = 0$

**Stationary Solutions.** For a symmetric BJJ, i.e.,  $\Delta E = 0$ , the equations of motion Eq. 2.6 are

$$\dot{z}(t) = -\sqrt{1 - z^2(t)} \sin(\phi(t)), \quad (4.1a)$$

$$\dot{\phi}(t) = \Lambda z(t) + \frac{z(t)}{\sqrt{1 - z^2(t)}} \cos(\phi(t)), \quad (4.1b)$$

with the conserved energy:

$$H_0 = H(z(0), \phi(0)) = \frac{\Lambda z(0)^2}{2} - \sqrt{1 - z(0)^2} \cos \phi(0). \quad (4.2)$$

The ground state solution of the symmetric BJJ, Eq. (4.1), is a symmetric eigenfunction of the GPE with energy  $E_+ = -1$  and:

$$\phi_s = 2n\pi \quad (4.3a)$$

$$z_s = 0 \quad (4.3b)$$

The next stationary state at higher energy  $E_- = 1$ , is an antisymmetric eigenfunction with:

$$\phi_s = (2n + 1)\pi \quad (4.4a)$$

$$z_s = 0 \quad (4.4b)$$

For non-interacting atoms in a symmetric double-well potential, the eigenstates of the Schrödinger equation are always symmetric or antisymmetric, with  $z_s = 0$ . However, because of the nonlinear interatomic interaction, there is a class of degenerate GPE eigenstates that break the  $z$  – *symmetry*:

$$\phi_s = (2n + 1)\pi \quad (4.5a)$$

$$z_s = \pm \sqrt{1 - \frac{1}{\Lambda^2}} \quad (4.5b)$$

provided that  $|\Lambda| > 1$ . The energy for this state is  $E_{sb} = \frac{1}{2} \left( \Lambda + \frac{1}{\Lambda} \right)$ .

These  $z$ -symmetry breaking states are an artifact of the semiclassical limit in which the GPE has been derived. In a full quantum two mode approximation the eigenstates are always symmetric in the population imbalance: as we will discuss later, such states have a large lifetime that scales exponentially with the total number of atoms.

**Rabi Oscillations.** For noninteracting atoms ( $\Lambda = 0$ ) Eqs. (4.1) describe sinusoidal Rabi oscillations between the two traps with frequency  $\omega_R = \frac{2}{\hbar} \mathcal{K}$ . These oscillations are equivalent to single atom dynamics, rather than a Josephson-effect arising from the interacting superfluid condensate. The possibility to tune the scattering length to values very close to zero [7], open avenues for their experimental observation.

**Zero-phase modes.** These modes describe the intra-well atomic tunneling dynamics with a zero time-average value of the phase across the junction,  $\langle \phi(t) \rangle = 0$ , and  $\langle z \rangle = 0$ . To this dynamical class belong small and large amplitude condensate oscillations.

*Small amplitude oscillations.* The small amplitude, or “plasma” (in analogy with SJJ), effect follows at once from the pendulum analogy. From Eq. (4.1), the BJJ is like a *non-rigid* pendulum of length

$$(x^2 + y^2)^{1/2} = \sqrt{1 - z^2} \quad (4.6)$$

decreasing with angular momentum  $z$ , and with moment of inertia  $\Lambda^{-1}$ . Linearizing Eq. (4.1), we obtain sinusoidal oscillations with inverse periods (in unscaled units)

$$\tau_L^{-1} = \sqrt{2UN_T\mathcal{K} + (2\mathcal{K})^2/2\pi\hbar}, \quad (4.7)$$

independent of the initial conditions  $z(0), \phi(0)$ . The comparison between Eq. (4.7) and Eq. (3.3) indicates that  $2N_T\mathcal{K}$  ( $\sim N_T$ ) is the analog of the Josephson coupling energy  $E_J$ , while  $U$  ( $\sim N_T^{-d/5}$ , with  $d$  the dimensionality of the system) is the analog of the capacitive

energy  $E_C$ . Since the coupling energy, fixed by the laser profile, is  $\mathcal{K} \sim A$ , the tunnel junction area whereas the bulk interaction,  $UN_T$ , is independent of  $A$ , the oscillation rate goes as  $\tau_L^{-1} \sim A^{1/2}$ . (The plasma frequency for SJJ,  $\tau_p^{-1} \sim \sqrt{E_c E_J}$  by contrast, is independent of  $A$ , as  $E_J \sim A, E_c \sim A^{-1}$ ).

The Josephson-like length ‘ $\lambda_J$ ’  $\equiv \sqrt{\hbar^2/2m\mathcal{K}}$ , that governs spatial variation along the junction, should be much greater than  $\sim \sqrt{A}$  to justify neglect of spatial variations of  $z, \phi$ , i.e., to obtain a ‘flat plasmon’ spectrum. For  $\mathcal{K} = 0.1\text{nK}$ , one finds ‘ $\lambda_J$ ’  $\sim 10\mu\text{m}$ . We will not, however, consider such spatial variations here. The frequency of the small amplitude oscillations in BJJ are of the order of 10 – 100 Hz for typical trap parameters, and should be compared with the frequencies of plasma SJJ that are of the order of GHz.

*Large amplitude oscillations.* In Fig. 2 we display this regime of anharmonic oscillations, plotting  $z = \frac{N_1 - N_2}{N_T}$  as a function of time, with the initial value of the phase difference  $\phi(0) = 0$  and  $\Lambda = 10$ , and for increasing values of the initial population imbalance  $z(0)$ . Specifically,  $z(0)$  takes on the values 0.1, 0.5, 0.59, 0.6, and 0.65 from a) through e) respectively. Increasing  $z(0)$  for fixed  $\Lambda$ , (or increasing  $\Lambda$  for fixed  $z(0)$ ) adds higher harmonics to the sinusoidal oscillations, corresponding to large amplitude oscillations of the (non-rigid) pendulum. This is shown in Fig. 2 (b,c). The period of such oscillations increases with  $z(0)$ , then decreases, undergoing a critical slowing down (Fig. 2(d), dashed line), with a logarithmic divergence. The singularity in the period corresponds to the pendulum in a vertically upright position, i.e., reaching the fixed point of Eq. (4.4b).

**Running-phase modes: Macroscopic Quantum Self-Trapping.** In addition to anharmonic and critically slow oscillations, other striking effects occur in BJJ. For instance, for a fixed value of the initial population imbalance, if the self-interaction parameter  $\Lambda$  exceeds a critical value  $\Lambda_c$ , the populations become macroscopically self-trapped with  $\langle z \rangle \neq 0$ . There are different ways in which this state can be achieved and all of them correspond to the condition (which we shall term the MQST condition) that

$$H_0 \equiv H(z(0), \phi(0)) = \frac{\Lambda}{2} z(0)^2 - \sqrt{1 - z(0)^2} \cos(\phi(0)) > 1 \quad (4.8)$$

In a series of experiments in which  $\phi(0)$  and  $z(0)$  are kept constant but  $\Lambda$  is varied (by changing the geometry or the total number of condensate atoms, for example), the critical parameter for MQST is

$$\Lambda_c = \frac{1 + \sqrt{1 - z(0)^2} \cos(\phi(0))}{z(0)^2/2}. \quad (4.9)$$

On the other hand, changing the initial value of the population imbalance  $z(0)$  with a fixed trap geometry and total number of condensate atoms (and initial value  $\phi(0)$ ),  $\Lambda$  remains constant and Eq. (4.8) defines a critical population imbalance  $z_c$ . As we shall see in this and the next section, for  $\phi(0) = 0$ , if  $z(0) > z_c$ , MQST sets in, but for  $\phi(0) = \pi$ ,  $z(0) < z_c$  marks the region of MQST. More generally, if  $|\phi(0)| \leq \pi/2$ , MQST occurs for  $z(0) > z_c$  while for other values of  $\phi(0)$ , it occurs for  $z(0) < z_c$ .

In this section, we will discuss the type of MQST in which the phase difference of the order parameter across the BJJ runs without bound; other types are discussed later. The phenomenon can be understood through the pendulum analogy. If the population imbalances are prepared such that the initial ‘angular kinetic energy’ of the pendulum,  $z^2(0)$ , exceeds the potential energy barrier height of the vertically displaced  $\phi = \pi$  ‘pendulum orientation’, there will occur a steady self-sustained ‘pendulum rotation’, with nonzero angular momentum  $\langle z \rangle$ , and a closed-loop trajectory around the pendulum support. For  $H_0 < 1$  the population imbalance oscillates about a zero value. For  $H_0 > 1$  the time-averaged ‘angular momentum’ is nonzero,  $\langle z(t) \rangle \neq 0$ , with oscillations around this nonzero value (Fig. 2). MQST is a nonlinear effect arising from the self-interaction  $\sim UN_T z^2$  of the atoms. It is dependent on the trap parameters, total number of atoms, and initial conditions, and is self-maintained in a closed conservative system without external drives. Although the SJJ ‘ac’ effect in the RCSJ model involves a running-phase, it is clearly physically different from MQST, as it is a driven steady-state independent of initial conditions. Moreover, in SJJ the Cooper pair population imbalance are locked to zero by the external circuit. MQST differs from single-electron Coulomb blockade effect that involves a single electron. It also differs from the self-trapping of polarons [32] that arise from single electrons interacting with a polarizable

lattice: arising, instead, from self-interaction of a *macroscopically large*, number of coherent atoms.

**$\pi$ -phase modes** These modes describe the tunneling dynamics in which the time-averaged value of the phase across the junction is  $\langle\phi\rangle = \pi$ .

The modes arise once more from the non-rigidity (momentum dependent length) of the pendulum and are not observable with SJJ. They include small amplitude, large amplitude, and macroscopic self-trapped oscillations. The last has nonzero average population imbalance, while  $\langle z \rangle = 0$  for the others. We summarize this behavior in the temporal evolution of  $z(t)$  in Fig. 3 for  $z(0) = 0.6, \phi(0) = \pi$ .  $\Lambda$  takes the values 0.1, 1.1, 1.111, 1.2, 1.25, and 1.3 in Figs. 3(a-f) respectively.

*Small amplitude oscillations.* For small  $z$ , Eqs. (4.1) can be linearized around the fixed point (4.4b) yielding harmonic oscillations for  $\Lambda < 1$ , with a period (in unscaled units):

$$\tau_{\pi}^{-1} = \sqrt{(2\mathcal{K})^2 - 2UN_T\mathcal{K}/2\pi\hbar}. \quad (4.10)$$

It is worth noticing that the ratio of the frequency of the small amplitude zero- and  $\pi$ - mode phase oscillations is  $\frac{\tau_L}{\tau_{\pi}} = \sqrt{\frac{1-\Lambda}{1+\Lambda}} < 1$  (similar to the  $^3\text{He-B}$   $\pi$ -oscillations of Section III).

Linearizing Eqs. (4.1) in  $z$  only, the BJJ Eq. (4.1b) reduces to the very simple form:

$$\ddot{\phi} = -[\Lambda \sin(\phi) + \frac{1}{2} \sin(2\phi)] + O(z^2) \quad (4.11)$$

This suggests a mechanical analogy in which a particle of spatial coordinate  $\phi$  moves in the potential:

$$V(\phi) = -\Lambda \cos(\phi) - \frac{1}{4} \cos(2\phi) + O(z^2) \quad (4.12)$$

In Fig. 4 we see that  $V(\phi)$  has a small valley around  $\phi = \pi$  where the particle can oscillate. The depth of this valley decreases as  $\Lambda \rightarrow 1$ . The valley persists, in the full potential for  $V(\phi)$ , retaining all the higher order terms in  $z$ .

*Large amplitude oscillations* For  $\pi$ -phase oscillations, the momentum dependent length allows the pendulum bob to make inverted anharmonic oscillations with  $\langle z \rangle = 0$  around the

(top of the) vertical axis. For large amplitude  $z(t)$  oscillations,  $\Lambda$  can exceed unity, as shown in Fig. 3(b).

*oscillations with macroscopic quantum self-trapping* Here the non-rigidity allows the penulum bob to make a closed  $\langle z \rangle \neq 0$  rotation loop around the top of the vertical axis. There are two kinds of such  $\pi$ -phase modes with MQST: those where the time average  $\langle z \rangle < |z_s| \neq 0$ , and those where  $\langle z \rangle > |z_s| \neq 0$ , with  $z_s$  being the stationary  $z$ -symmetry breaking value of the GPE. These two kinds of MQST are shown in the time evolution of  $z(t)$  in Figs. 3(d-f). In Fig. 3(d), the system is in the first type of trapped state. A change over occurs at the stationary state (Fig. 3(e), dashed line). Once  $\Lambda$  exceeds this value  $\Lambda_s = 1/\sqrt{1 - z(0)^2}$  (cf. Eq. 4.5), the system goes into the second type of  $\pi$ -phase trapped state (Fig. 3(f)).

In order to see these different kinds of (running- and  $\pi$ -phase) MQST modes more transparently, one can use the energy  $H = H_0$  of Eq. (4.2) to write the system of equations (4.1) in terms of an equation of motion of a classical particle whose coordinate is  $z$ , moving in a potential  $W(z)$  with total energy  $W_0$ ,

$$\dot{z}(t)^2 + W(z) = W_0, \quad (4.13a)$$

where

$$W(z) = z^2 \left( 1 - \Lambda H_0 + \frac{\Lambda^2}{4} z^2 \right); \quad W_0 = W(z(0)) + \dot{z}(0)^2 \quad (4.13b)$$

Figure 5 displays the potential  $W(z)$  against  $z$  (Figs. 5(a) and (c)) and the corresponding evolution of  $\phi(t)$  (Figs. 5 (b) and (d)) to display the various dynamical regimes. In Fig. 5(a) and (b)  $\phi(0) = 0, \Lambda = 10$  and in Fig. 5 (c) and (d)  $\phi(0) = \pi, \Lambda = 2.5$ . The horizontal lines indicate the energy value  $W_0$ . For fixed value of  $\Lambda$ , and  $\phi(0) = 0$ , increasing the value of  $z(0)$  changes  $W(z)$  from a parabolic to a double-well. The motion of the particles lies within the classical turning points in which the total energy equals the potential energy. For  $z(0) = 0.1$ , in Fig. 5(a), the potential is parabolic, and the (small amplitude) oscillations are sinusoidal. For  $z(0) = 0.6$  the trajectory of  $z(t)$  becomes markedly nonsinusoidal, given the



double-well structure of  $W(z)$ . For  $z(0) \geq 0.6$  the total energy is smaller than the potential barrier, forcing the particle to become localized in one of the two wells. The symmetry of the classical motion is broken. This corresponds to an MQST state. Figure 5(b) displays the corresponding phase  $\phi = \arccos[(\Lambda z^2/2 - H_0)/\sqrt{1 - z^2}]$  versus  $z$ . For untrapped oscillations, the  $\phi, z$  trajectory is a closed curve, with a time-averaged value of  $\phi(t) = 0$ . In the running-mode MQST regime  $-\infty < \phi(t) < \infty$ . for the corresponding  $\phi$  evolution.

Let us now focus our attention on Figs. 5(c,d). For  $\Lambda = 2.5, \phi(0) = \pi$ , the  $z$ -potential always has a double-well structure and the system is self-trapped for all values of  $z(0)$ . For small values of  $z(0)$ , the phase  $\phi(t)$  is unbounded and the system exhibits running-phase MQST. However, above a certain value of  $z(0) = 2z_s = 2\sqrt{1 - 1/\Lambda^2}$ , the phase  $\phi(t)$  becomes localized around  $\pi$  and remains bounded for all larger values of  $z(0)$ . In Fig. 5(c,d),  $z(0) = 0.7$  and  $0.98$  mark the two different kinds of  $\pi$ -phase MQST since they are on either side of the stationary state value of  $z_s = \sqrt{1 - 1/\Lambda^2}$ . This point will become more clear in the phase-plane portrait of Fig. 7.

**Discussion of Results.** A clear observational feature of the behavior of the system is the time-period of oscillations. To this end, we plot in Fig. 6, the inverse period  $1/\tau$  as a function of the ratio between the initial population imbalance  $z(0)$  and the critical population imbalance  $z_c$ . Figure 6(a) shows the case for  $\phi(0) = 0$  and  $\Lambda = 10(z_c = 0.6)$  (dashed line) and  $\Lambda = 100(z_c = 0.2)$  (solid line). The initial parts of the graph for  $z(0) \ll z_c$  mark sinusoidal small amplitude ('plasma') oscillations (Fig. 2(a)). On increasing  $z(0)$ , the oscillations become highly anharmonic, with the inverse period that first increases, then decreases, displaying a critical slowing down. The logarithmic divergence of the time-period at  $z(0) = z_c$  is marked by the hyperbolic secant evolution of  $z(t)$  (Fig. 2(d)). In the inset, we show the average value,  $\langle z \rangle$ , as a function of  $z(0)/z_c$ . MQST is signaled by the sharp ('phase-transition'-like) rise of  $\langle z \rangle$  from zero to a non-zero value. For  $\phi(0) = \pi$ , Fig. 6(b), something different happens. MQST occurs for values of the initial imbalance  $z(0)$  less than  $z_c$ . At  $z(0) = z_c$  the time-period diverges, and for larger values of  $z(0)$ , MQST disappears.

The dynamical behavior of the BJJ system can be summarized quite conveniently in

terms of a phase portrait of the two dynamical variables  $z$  and  $\phi$ , as shown in Fig. 7. The trajectories are calculated for different values of  $\Lambda/\Lambda_c$  with  $z(0)$  kept constant at 0.6. The light solid lines mark the evolution where the phase  $\phi$  oscillates around 0 and  $\langle z \rangle = 0$ . The running mode MQST is shown by the trajectories with small dots for  $\Lambda/\Lambda_c = 1, 1.5$  with the initial condition being  $\phi(0) = 0$ . Note that for a rigid pendulum (without the  $\sqrt{1-z^2}$  term in the Hamiltonian in Eq. (2.8)), one would obtain only the curves described thus far. However, for the BJJ, due to the momentum dependent potential in Eq. (2.8), there is considerable richness as exhibited by the dark solid lines, dashed lines, and lines with large dots. All these curves correspond to  $\phi(0) = \pi$ . Note, for instance, that as  $\Lambda/\Lambda_c$  increases and approaches unity, the area enclosed by the trajectory shrinks and is pinched at  $\Lambda = \Lambda_c$  marking the onset of  $\pi$ -phase MQST with  $\langle z \rangle < |z_s|$  (dashed line). Upon further increase, the area collapses to a point at the  $z = z_s$  stationary  $z$ -symmetry breaking state. Further increase of  $\Lambda/\Lambda_c$  induces a reflection of the trajectory about the fixed point, and  $\pi$ -phase MQST with  $\langle z \rangle > |z_s|$  (lines with large dots). Finally, the trajectories join the running mode MQST for  $\Lambda/\Lambda_c = 2.7$  (lines with small dots).

We now outline a possible procedure for a) bridging experimental data with our theoretical model, and b) collapsing data from different experiments onto a single universal curve. We note, at the very outset, that other procedures could be experimentally more accessible, particularly since novel methods of tailoring traps [3] and the possibility of tuning the scattering length of atoms [7] have become current. The calculation of the values of  $\Lambda$  and  $\mathcal{K}$  from the experimental data (for a given trap geometry and total number of condensate atoms) is straightforward. The onset of MQST is provided by Eq. (4.9), which immediately gives the value of  $\Lambda_c$  from the (experimentally imposed) initial conditions  $z(0)$  and  $\phi(0)$ . Moreover, in the small amplitude limit the inverse period of the oscillations, given by Eq.(4.7), provides the value of  $\mathcal{K}$  from the previously calculated  $\Lambda$ .

Different experiments done by varying arbitrarily the trap geometry and the number of condensate atoms give a set of parameters  $\Lambda, \mathcal{K}$ . The data collapse onto a single universal curve of  $\pi/(\mathcal{K}C\Lambda^2\tau)$  versus  $k^2(\Lambda)$  of Eq. (B7), as shown in Fig. 8.

The parameters  $UN_T$ , and  $E^0$  can be estimated to be  $\sim 100\text{nK}$  and  $\sim 10\text{nK}$  respectively for  $N_T = 10^4$  if we take the trap-frequency  $\omega_{trap}$  to be  $\sim 100\text{Hz}$ .  $\Lambda = UN_T/2\mathcal{K}$  can be varied widely by changing  $N_T$  or the barrier height  $\sim \mathcal{K}$  that depends exponentially on the laser-sheet thickness. Typical frequencies are then  $1/\tau_L \sim 100\text{Hz}$ . With collective mode excitation energies  $\Delta_{coll} \sim E^0$ , and quasiparticle gaps  $\Delta_{qp} \sim \sqrt{UN_TE^0}$ , for  $UN_T z < \Delta_{qp,coll}$  intra-well excitations are not induced. At nonzero temperatures, BEC depletion and thermal fluctuations will renormalize the parameters in Eq. (2.7), and will damp [18] the coherent oscillations. The effects of damping on the oscillation behaviour requires a separate treatment and will be considered elsewhere.

## V. THE ASYMMETRIC TRAP CASE, $\Delta E \neq 0$

**Exact solutions and temporal behavior.** Let us now consider the case where the traps are asymmetric, i.e.,  $\Delta E \neq 0$ , as in Fig. 1, with Hamiltonian

$$H = \frac{\Lambda z^2}{2} + \Delta E z - \sqrt{1 - z^2} \cos \phi. \quad (5.1)$$

For  $\Lambda z(0) \ll \Delta E$ , the non-rigid pendulum is driven to rotate in a direction determined by  $\Delta E$  (corresponding to the ac Josephson-like effect). With  $\Delta E = 0$ , and  $\Lambda > \Lambda_c$  (of Eq. (4.9), we had found that the pendulum also executes rotatory motion, in a direction determined by  $z(0)$ . For  $\Lambda z(0) \gg \Delta E \neq 0$ , we expect this type of motion to persist (corresponding to MQST due to nonlinearity). In between there should be competition between the two effects, and a transition at some shifted critical value  $\Lambda = \Lambda_c(\Delta E)$ . This physical picture for  $\Delta E \neq 0$  is confirmed by obtaining  $z(t)$  in terms of Weierstrassian elliptic functions that change their behavior at a singular value  $\Lambda = \Lambda_c(\Delta E)$ .

We show in Figs. (9) that the MQST phenomena, (inverse-period dip, average non-zero imbalance), persist in the  $\Delta E \neq 0$  case, and display dependence on  $\Lambda$  and  $\Delta E$ . Figure 9 shows the scaled inverse period  $\tau_{ac}/\tau$  versus the scaled nonlinearity ratio  $\Lambda/\Lambda_c(\Delta E)$  where  $\tau_{ac}$  is as in Eq. (4.7), with  $z(0) = 0.1$ ,  $\Delta E = 1.0$ , and  $\phi(0) = 0, \pi$ . The dip to zero at

the onset of MQST is clearly seen. The inset shows the time-averaged  $\langle z \rangle$  for  $\phi(0) = 0, \pi$ , vanishing at  $\Lambda = \Lambda_c(\Delta E)$ . Whereas for  $\Delta E = 0$  and  $\Lambda < \Lambda_c(\Delta E = 0)$ , the average population imbalance was zero, for  $\Delta E \neq 0$  we have  $\langle z \rangle \neq 0$  in the corresponding subcritical region  $\Lambda < \Lambda_c(\Delta E)$ . This is analogous to a voltage across a capacitor inducing a charge difference and the external static magnetic field in the case of  $^3\text{He-A}$ . Note that there is a combined influence of  $\Lambda, \Delta E, \phi(0)$ , so  $\langle z \rangle$  can be larger (in magnitude) than  $z(0)$ . In particular, for  $\Lambda \rightarrow 0$ ,  $\langle z \rangle \rightarrow -\Delta E(\sqrt{1 - z^2(0)} \cos \phi(0) - \Delta E z(0))/(1 + \Delta E^2)$ , that for  $\phi(0) = 0$  is negative, as in the inset. This corresponds to an averaged pendulum rotation  $\langle z \rangle \sim -\Delta E < 0$ , opposite in sign to the initial  $z(0) > 0$ , but slowing to zero as the critical value is approached. For  $\Lambda > \Lambda_c(\Delta E)$ , in the MQST regime, the averaged rotation  $\langle z \rangle > 0$  is in the initial direction of  $z(0) > 0$ , with  $\langle z \rangle$  approaching the initial  $z(0)$  value for large  $\Lambda$ , as in the  $\Delta E = 0$  case of Fig. 8.

**Shapiro Effect Analogs.** Let us now consider the BJJ analog of the Shapiro resonance effect observed in SJJ [23]. In addition to a time-independent trap asymmetry  $\Delta E$ , we impose a sinusoidal variation so that we can write the asymmetry term as  $\Delta E + \Delta E_1 \cos \omega_0 t$ . This could be done by varying the laser barrier position at fixed intensity. A similar Shapiro-like resonance effect could be seen, with an oscillation of the laser beam intensity, at fixed mid-position, so  $\mathcal{K} \rightarrow \mathcal{K}(1 + \delta_0 \cos \omega_0 t)$ . The analog of the Shapiro effect arises when the period from the time independent asymmetry,  $\sim 1/\Delta E$ , matches that from the oscillatory increment,  $\sim 1/\omega_0$ . This matching condition is intimately connected with the phenomenon of Bloch oscillations and dynamic localization in crystals and trapping in two-level atoms [38]. The dc value of the drift current,  $\langle \dot{z}(t) \rangle$ , as a function of  $\Delta E$ , will show up as resonant spikes. (For SJJ, with current drives, the Shapiro effect shows up as steps in the I-V characteristics.) Of course, the dc drift cannot persist indefinitely, because the phase difference between the condensates on the two parts of the BJJ will cease to be a well-defined quantity once the population in one well drops below  $N_{min}$ .

Figure 10 shows  $I_{dc} \propto \langle \dot{z}(t) \rangle$  obtained from time averaging the numerical solution, with a small ac drive and  $\Delta E \neq 0$ . It is plotted as a function of  $\Delta E/\omega_0$  for increasing values

of the nonlinearity ratio  $\Lambda$ . The initial conditions are  $z(0) \sim 0 = 0.045$ ,  $\phi(0) = \pi/2$ , for which  $\Lambda_c \sim 1000$  (in the absence of  $\Delta E$  and ac driving). When  $\Lambda$  is zero, sharp peaks in  $I_{dc}$  occur at the usual ‘Shapiro’ condition values  $\Delta E \propto n\omega_0$ ,  $n = 1, 2, \dots$ . As  $\Lambda$  increases, however, two things happen. Firstly, multiple peaks also occur at  $\Delta E/\omega_0$  values different from integers. Close to the MQST regime, ( $\Lambda \sim \Lambda_c$ ), there is a proliferation of peaks as the system moves from a regime of constant current,  $\langle \dot{z} \rangle \neq 0$  ( $\Lambda$  small), to one of constant population imbalance  $\langle z \rangle \neq 0$  ( $\Lambda$  large). Secondly, the magnitude of the peaks or dc currents decreases.

Finally, we note that for  $\Delta E$  larger than the Bogoliubov quasiparticle gap  $\Delta_{qp}$ , and high enough temperatures, a dissipative quasiparticle branch might be observable.

## VI. SUMMARY

We have investigated the Josephson dynamics in two weakly linked Bose-Einstein condensates forming a Boson Josephson junction. In the resulting nonlinear two-mode model, we have described the temporal oscillations of the population imbalance of the condensates in terms of elliptic functions. Our predictions include non-sinusoidal generalizations of Josephson ‘dc’, ‘ac’ and Shapiro effects. We also predict macroscopic quantum self-trapping which is a self-maintained population imbalance across the junction due to atomic self-interaction, and  $\pi$ -oscillations, in which the phase difference across the junction oscillates around  $\pi$ . We clarify the connection and the differences between these phenomena and others occurring in related systems like the superconducting Josephson junctions, the internal Josephson effect in  $^3\text{He-A}$ , and Josephson oscillations between two weakly linked reservoirs of  $^3\text{He-B}$ . Through a set of functional relations, we also predict the collapse of experimental data (corresponding to different trap geometries and total number of condensate atoms) onto a single universal curve. These effects constitute experimentally testable signatures of quantum phase coherence and the superfluid character of weakly interacting Bose-Einstein condensates.

Discussions with V. Chandrasekhar, S. Giovanazzi, L. Glazman, A. J. Leggett, E. Tosatti and useful references from G. Williams are acknowledged.

## APPENDIX A: MICROSCOPIC DERIVATION OF THE BOSON JOSEPHSON EQUATION FROM THE GROSS-PITAEVSKII EQUATION

The values of the constant parameters in BJJ Eqs. (2.3)  $\mathcal{K}$ ,  $E_0$ , and  $U$  depend on the geometry (and effective dimensionality) of the system and the total number of condensate atoms. We now outline their dependence in term of spatial GPE wave functions, elucidating the approximations underlying the BJJ equations.

We look for the solution of the (time-dependent) GPE (2.1) with the following *variational* ansatz:

$$\Psi(r, t) = \psi_1(t)\Phi_1(r) + \psi_2(t)\Phi_2(r) \quad (\text{A1})$$

There are two approximations underlying this ansatz:

1. We describe the temporal evolution of the GP wave function as the *superposition* of two wave functions (roughly) describing the condensate in each trap. The nonlinear interaction in GPE destroys such superposition. In effect if the condensate density in the tunneling region is small (as it is the case for weak links) nonlinear interaction in that region is negligible, and the superposition ansatz is preserved.
2. We factorize the temporal and the spatial dependence of the GPE wave function describing the condensate in each trap. Later in this section, we will discuss the limit of validity of this approximation.

The spatial dependence of  $\Phi_{1,2}(r)$  can be constructed by the exact symmetric  $\Phi_+(r)$  and antisymmetric  $\Phi_-(r)$  stationary eigenstates of the GPE (see Section IV):

$$\Phi_1(r) = \frac{\Phi_+ + \Phi_-}{2} \quad (\text{A2a})$$

$$\Phi_2(r) = \frac{\Phi_+ - \Phi_-}{2} \quad (\text{A2b})$$

ensuring that:

$$\int \Phi_1(r)\Phi_2(r)dr = 0 \quad (\text{A3})$$

and where we impose the normalization condition:

$$\int |\Phi_{1,2}(r)|^2 dr = 1 \quad (\text{A4})$$

Replacing Eqs. (A1,A2) in the GPE (2.1), and using the orthogonality condition Eq. (A3), we obtain the BJJ equations,

$$i\hbar \frac{\partial \psi_1}{\partial t} = (E_1^0 + U_1 N_1) \psi_1 - \mathcal{K} \psi_2 \quad (\text{A5a})$$

$$i\hbar \frac{\partial \psi_2}{\partial t} = (E_2^0 + U_2 N_2) \psi_2 - \mathcal{K} \psi_1, \quad (\text{A5b})$$

with constant parameters :

$$E_0 = \int \frac{\hbar^2}{2m} |\nabla \Psi|^2 + |\Psi|^2 V_{ext}(r) dr \quad (\text{A6a})$$

$$U = g_0 \int |\Psi|^4 dr \quad (\text{A6b})$$

$$\mathcal{K} \simeq - \int \left[ \frac{\hbar^2}{2m} (\nabla \Psi_1 \nabla \Psi_2) + \Psi_1 V_{ext} \Psi_2 \right] dr \quad (\text{A6c})$$

We now return to our variational ansatz  $\Psi(r, t) = \psi_1(t)\Phi_1(r) + \psi_2(t)\Phi_2(r)$ . The parameters  $U, \Delta E \sim$  wave-function overlaps are  $N_T$ -dependent, but are independent of  $z(t)$ , so the chemical potential difference is considered linear in  $z$ . This approximation captures the dominant  $z$ -dependence of the tunneling equations coming from the scale factors  $\psi_{1,2} \propto \sqrt{N_{1,2}}$ , but ignores shape changes in the wavefunctions for  $N_1(t) \neq N_2(t)$ . We can estimate such corrections to the chemical potential difference  $\Delta\mu \equiv \mu_1 - \mu_2$ , within the Thomas-Fermi approximation  $\mu_{1,2} \sim N_{1,2}^{2/5} \sim (N_T/2)^{2/5} (1 \pm z)^{2/5}$ . Then relative corrections to the linear form  $\Delta\mu = (4/5)z$  are estimated by  $\mathcal{E} \equiv (\Delta\mu(z) - 4z/5)/\Delta\mu(z)$  where  $\Delta\mu(z) = (1+z)^{2/5} - (1-z)^{2/5}$ . We find that  $\mathcal{E}$  is negligible over the  $z$  range where MQST effects are expected:  $\mathcal{E} \sim 0.1\%$  for  $z = 0.1$  and  $\mathcal{E} \sim 3\%$  for  $z = 0.4$ . Thus Eq. (2.6) with  $\Delta E, \Lambda$  treated as constants, is indeed a reliable nonlinear equation describing BJJ dynamics for a large range of  $z(t)$  values. Similar conclusions has been reached in [18]. As a further test,

the GPE (2.1) has been solved numerically (in a spatial grid) in the double well geometry [39], fully confirming the conclusions just outlined.

## APPENDIX B: EXACT SOLUTIONS IN TERMS OF JACOBIAN ELLIPTIC FUNCTIONS

The total energy of the system is given by

$$H(z(t), \phi(t)) = \frac{\Lambda z^2}{2} + \Delta E z - \sqrt{1 - z^2} \cos \phi = H(z(0), \phi(0)) \equiv H_0, \quad (\text{B1})$$

where  $H_0$  is the initial (and conserved) energy. Combining Eqs. (2.6a),(2.8), we have

$$\dot{z}^2 + \left[ \frac{\Lambda z^2}{2} + \Delta E z - H_0 \right]^2 = 1 - z^2. \quad (\text{B2})$$

The nonlinear GPE tunneling equations for the macroscopic amplitudes  $\psi_1(t), \psi_2(t)$  are formally identical to equations governing a physically very different problem — a single electron in a polarizable medium, forming a polaron [32]. Solutions have been found [32,40–42], for the discrete nonlinear Schrödinger equation (DNLSE) describing the motion of the polaron between two sites of a dimer. Similarly, we use Eq. (B2) to obtain the exact solution for  $z(t)$  in terms of quadratures,

$$\frac{\Lambda t}{2} = \int_{z(t)}^{z(0)} \frac{dz}{\sqrt{\left(\frac{2}{\Lambda}\right)^2 (1 - z^2) - \left[z^2 + \frac{2z\Delta E}{\Lambda} - \frac{2H_0}{\Lambda}\right]^2}} \quad (\text{B3})$$

We consider  $\Delta E = 0$ , and  $\Delta E \neq 0$  cases separately. For symmetric double wells,  $\Delta E = 0$ , the denominator of Eq. (B3) can be factorized, so

$$\frac{\Lambda t}{2} = \int_{z(t)}^{z(0)} \frac{dz}{\sqrt{(\alpha^2 + z^2)(C^2 - z^2)}}, \quad (\text{B4})$$

where

$$C^2 = \frac{2}{\Lambda^2} \left[ (H_0\Lambda - 1) + \frac{\zeta^2}{2} \right]; \quad \alpha^2 = \frac{2}{\Lambda^2} \left[ \zeta^2 - (H_0\Lambda - 1) \right], \quad (\text{B5a})$$

$$\zeta^2(\Lambda) = 2\sqrt{\Lambda^2 + 1 - 2H_0\Lambda}. \quad (\text{B5b})$$



The solution to Eq. (B4) is written in terms of the ‘cn’ and ‘dn’ Jacobian elliptic functions, (with  $k$ , the elliptic modulus [43]) as

$$z(t) = C \operatorname{cn}[(C\Lambda/k)(t - t_0), k] \text{ for } 0 < k < 1$$

$$= C \operatorname{dn}[(C\Lambda)(t - t_0), 1/k] \text{ for } k > 1; \quad (\text{B6a})$$

$$k^2 = \frac{1}{2} \left( \frac{C\Lambda}{\zeta(\Lambda)} \right)^2 = \frac{1}{2} \left[ 1 + \frac{(H_0\Lambda - 1)}{\sqrt{\Lambda^2 + 1 - 2H_0\Lambda}} \right], \quad (\text{B6b})$$

$$t_0 = 2[\Lambda\sqrt{C^2 + \alpha^2}F(\arccos(z(0)/C), k)]^{-1}, \quad (\text{B6c})$$

where  $F(\phi, k) = \int_0^\phi d\phi (1 - k^2 \sin^2 \phi)^{-1/2}$  is the incomplete elliptic integral of the first kind.

The Jacobian elliptic functions  $\operatorname{cn}(u, k)$  and  $\operatorname{dn}(u, k)$  are periodic in the argument  $u$  with period  $4K(k)$  and  $2K(k)$  respectively where  $K(k) \equiv F(\pi/2, k)$  is the complete elliptic integral of the first kind. The character of the solution changes when elliptic modulus  $k = 1$ . From Eq. (B6b), this mathematical condition or singular parameter-dependence of the elliptic functions corresponds to the physical condition  $H_0 = 1, \Lambda = \Lambda_c$  of Eq. (4.9), for the onset of MQST:  $k^2(\Lambda_c) = 1$ . When  $k^2 \ll 1$ ,  $\operatorname{cn}(u, k) \approx \cos u + k^2 \sin u(u - \frac{1}{2} \sin 2u)$  is almost sinusoidal. When  $k^2$  increases, the departure from simple sinusoidal forms becomes drastic. For  $k^2 \lesssim 1$ ,  $\operatorname{cn}(u, k) \approx \operatorname{sech} u - \frac{1-k^2}{4}(\tanh u \operatorname{sech} u)(\sinh u \cosh u - u)$  becomes non-periodic. When  $k^2 \gg 1$ , the behavior is again periodic (but about a non-zero average):  $\operatorname{dn}(u, 1/k) \approx 1 - (\sin^2 u)/2k^2$ .

The time-period of oscillation of  $z(t)$  is given [43] by

$$\tau = \frac{4kK(k)}{C\Lambda} \text{ for } 0 < k < 1, \quad (\text{B7a})$$

$$= \frac{2K(1/k)}{C\Lambda} \text{ for } k > 1. \quad (\text{B7b})$$

In the linear limit,  $\tau \rightarrow \pi/\sqrt{1 + \Lambda}$  in agreement with the expression for  $\tau_p$  in Eq. (4.7). As  $k \rightarrow 1$ , or  $\Lambda \rightarrow \Lambda_c$ , the period becomes infinite, as in ‘critical slowing down’, diverging logarithmically,  $K(k) \rightarrow \log(4/\sqrt{1 - k^2})$ . The evolution of the imbalance is given, in this special case, by the non-oscillatory hyperbolic secant ( $C = 2\sqrt{\Lambda_c - 1}/\Lambda_c$ ):

$$z(t) = C \operatorname{cn}[(C\Lambda_c)(t - t_0), 1] = C \operatorname{sech} C\Lambda_c(t - t_0) \text{ for } k = 1. \quad (\text{B8})$$

We now turn to the  $\Delta E \neq 0$  case. The general form of the integral of Eq. (B3) is split into two parts,

$$\frac{\Lambda t}{2} = \frac{\Lambda t_0}{2} + \int_{z(0)}^{z_1} \frac{dz'}{\sqrt{f(z')}} \quad (\text{B9})$$

where  $\Lambda t_0/2$  is the integral from  $z_1$  to  $z(0)$ , and  $z_1$  is a root of the quartic  $f(z) = \left(\frac{2}{\Lambda}\right)^2 (1 - z^2) - \left[z^2 + \frac{2z\Delta E}{\Lambda} - \frac{2H_0}{\Lambda}\right]^2$ . Taylor expanding  $f(z)$  around  $z$ , and with the change of variable  $y = y(z) = (f'(z_1)/4)(z - z_1)^{-1} + f''(z_1)/24$  for which  $y(z_1) = \infty$ , the integral in Eq. (B9) is cast in a standard form

$$\frac{\Lambda(t - t_0)}{2} = \int_y^\infty \frac{dy'}{\sqrt{4y'^3 - g_2y' - g_3}}, \quad (\text{B10})$$

which can be inverted as a Weierstrassian elliptic function  $y = \wp(\Lambda(t - t_0)/2; g_2, g_3)$ . Thus

$$z(t) = z_1 + \frac{f'(z_1)/4}{\wp(\Lambda(t - t_0)/2; g_2, g_3) - f''(z_1)/24} \quad (\text{B11})$$

In Eq. (B10), the constants in the cubic  $h(y) = 4y^3 - g_2y - g_3$  are determined from the coefficients  $a_i$  of  $f(z) = \sum_{l=0}^4 a_{l+4}z^l$  as

$$g_2 = -a_4 - 4a_1a_3 + 3a_2^2; \quad g_3 = -a_2a_4 + 2a_1a_2a_3 - a_2^3 + a_3^2 - a_1^2a_4, \quad (\text{B12})$$

where

$$a_1 = -\frac{\Delta E}{\Lambda}; \quad a_2 = \frac{2}{3\Lambda^2}(\Lambda(H_0 + 1) - \Delta E^2); \quad a_3 = \frac{2H_0\Delta E}{\Lambda^2}; \quad a_4 = \frac{4(1 - H_0^2)}{\Lambda^2}, \quad (\text{B13})$$

The solution Eq. (B11) is equivalent to that found in polaronic [44] and other contexts [45,46], where  $\Delta E \neq 0$  corresponds to a difference or ‘disorder’ in on-site electronic or excitonic energies.

For  $\Delta E = 0$  we found that the elliptic modulus  $k^2$  governed the behavior of the Jacobian elliptic function solutions. For  $\Delta E \neq 0$ , the discriminant  $\delta = g_2^3 - 27g_3^2$  of the cubic  $h(y)$  (with roots  $y_{1,2,3}$ ) governs the behavior of the Weierstrassian elliptic functions [43] For  $\delta \neq 0$ , the solutions are oscillatory about a non-zero average,  $\langle z \rangle \neq 0$ . For  $\delta = 0$ ,  $\langle z \rangle = 0$ , and the time-period diverges, corresponding to  $\Lambda = \Lambda_c(\Delta E)$ , the onset of MQST.

The time-period of oscillation can be written in terms of complete elliptic integrals of the first kind  $K(k)$  as in the  $\Delta E = 0$  case of Eq. (B7). However, the argument and prefactors are different, with

$$\tau = K(k_1)/(y_1 - y_3), \text{ for } \delta > 0, \quad (\text{B14a})$$

$$\tau = K(k_2)/\sqrt{H_2}, \text{ for } \delta < 0, \quad (\text{B14b})$$

$$\tau = \infty, \text{ for } \delta = 0, g_3 \leq 0. \quad (\text{B14c})$$

For  $\delta > 0$ ,  $k_1^2 = (y_2 - y_3)/(y_1 - y_3)$  where the roots  $y_i$  of  $h(y)$  are all real,  $y_i = -\sqrt{g_2/3} \cos([\theta + 2\pi(i-1)]/3)$  and  $\theta = \arccos(\sqrt{27g_3^2/g_2^3})$ . For  $\delta = -|\delta| < 0$ ,  $k_2 = 1/2 - 3y_2/4(3y_2^2 - g_2)$  where  $y_2$  is the only real root,  $y_2 = [(g_3 + \sqrt{-\delta/27})^{1/3} + (g_3 - \sqrt{-\delta/27})^{1/3}]/2$ . Thus the inverse oscillation period  $1/\tau$ , for  $\delta \neq 0$ , is obtained as above in terms of  $\Lambda$  and  $\Delta E$ , with  $1/\tau = 0$  at  $\Lambda = \Lambda_c(\Delta E)$ .

## REFERENCES

- [1] S. N. Bose, Z. Phys. **26**, 178 (1924); A. Einstein, Sitzber. Kgl. Akad. Wiss., (1924), p.261; (1925), p.3; For a historical view, see also A. Pais, *Subtle is the Lord, The Science and the Life of Albert Einstein* (Clarendon Press, Oxford, 1982), Ch. 23.
- [2] M. H. Anderson, M. R. Matthews, C. E. Wieman, and E. A. Cornell, Science **269**, 198 (1995); K. B. Davis, M.-O. Mewes, M. R. Andrews, N. J. van Druten, D. S. Durfee, D. M. Kurn, and W. Ketterle, Phys. Rev. Lett. **75**, 3969 (1995); C. C. Bradley, C. A. Sackett, J. J. Tollett, and R. G. Hulet, Phys. Rev. Lett. **75**, 1687 (1995).
- [3] D. M. Stamper-Kurn *et al.*, Phys. Rev. Lett. **80**, 2027 (1998).
- [4] D. M. Stamper-Kurn *et al.*, cond-mat/9805022.
- [5] M. R. Andrews *et al.*, Science, **273**, 84 (1996) .
- [6] D. S. Hall *et al.*, cond-mat/9805327.
- [7] S. Inouye *et al.*, Nature **392**, 15 (1998).
- [8] A. J. Leggett and F. Sols, Foundations of Physics **21**, 353 (1991).
- [9] L. P. Pitaevskii, Sov. Phys. JETP, **13**, 451 (1961); E. P. Gross, Nuovo Cimento **20**, 454 (1961); J. Math. Phys. **4**, 195 (1963).
- [10] M. Edwards *et al.*, Phys. Rev. Lett. **77**, 1671 (1996); S. Stringari, Phys. Rev. Lett. **77**, 2360 (1996).
- [11] A. Smerzi and S. Fantoni, Phys. Rev. Lett. **78**, 3589 (1997).
- [12] Y. Kagan, E. L. Surkov, and G. V. Shlyapnikov, Phys. Rev. A **55**, R18 (1997).
- [13] R. J. Dodd *et al.* Phys. Rev. A **56**, 587 (1997); D. S. Rokhsar, Phys. Rev. Lett. **79**, 2164 (1997); M. Benakli, S. Raghavan, A. Smerzi, S. Fantoni, and S. R. Shenoy, submitted.
- [14] M. R. Andrews, C. G. Townsend, H.-J. Miesner, D. S. Durfee, D. M. Kurn, and W.

- Ketterle, *Science* **275**, 637 (1997).
- [15] D. S. Hall, M. R. Matthews, J. R. Ensher, C. E. Wieman, and E. . Cornell, *cond-mat/9804138*.
- [16] J. Javanainen, *Phys. Rev. Lett.* **57**, 3164 (1986).
- [17] F. Dalfovo, L. Pitaevskii, and S. Stringari, *Phys. Rev. A* **54**, 4213 (1996).
- [18] I. Zapata, F. Sols, and A. Leggett, *Phys. Rev. A* **57**, R28 (1998).
- [19] C. J. Milburn, J. Corney, E. M. Wright, and D. F. Walls, *Phys. Rev. A* **55**, 4318 (1997).
- [20] A. Imamoglu, M. Lewenstein, and L. You, *Phys. Rev. Lett.* **78**, 2511 (1997).
- [21] A. Smerzi, S. Fantoni, S. Giovannazzi, and S. R. Shenoy, *Phys. Rev. Lett.* **79**, 4950 (1997).
- [22] A. Barone and G. Paterno, *Physics and Applications of the Josephson Effect* (Wiley, New York, 1982); H. Ohta, in *SQUID: Superconducting Quantum Devices and their Applications*, edited by H. D. Hahlbohm and H. Lubbig (Walter de Gruyter, Berlin, 1977).
- [23] L. Solymar, *Superconductive tunnelling and applications* (Chapman and Hall, London, 1972).
- [24] M. Tinkham, *Introduction to Superconductivity*, 2<sup>nd</sup> ed. (McGraw-Hill, New York, 1996).
- [25] R. A. Webb, R. L. Kleinberg and J. C. Wheatley, *Phys. Lett* **48A**, 421 (1974); *Phys. Rev. Lett* **33**, 145 (1974).
- [26] A. J. Leggett, *Rev. Mod. Phys.* **47**, 331 (1975).
- [27] K. Maki and T. Tsuneto, *Prog. Theor. Phys.* **52**, 773 (1974).
- [28] S. Backhaus, S. V. Pereverzev, R. W. Simmonds, A. Loshak, J. C. Davis, and R. E. Packard, *Nature* **392**, 687 (1998).

- [29] M. H. Anderson, M. R. Matthews, C. E. Wieman, and E. A. Cornell, *Science* **269**, 198 (1995).
- [30] Including gravitational effects, the trap potential of Eq. (2.1) becomes  $V_{trap}(\mathbf{r}) = \frac{1}{2}m\omega_{trap}^2\mathbf{r}^2 - mgz = \frac{1}{2}m\omega_{trap}^2(\mathbf{r} - \mathbf{r}_g)^2 - \frac{1}{2}\frac{mg^2}{\omega_{trap}^2}$ , where the gravitational acceleration  $g$ , enters only as a ‘sag’ or unimportant shift of both the wavefunctions’ centers,  $\mathbf{r}_g = \left(0, 0, \frac{g}{\omega_{trap}^2}\right)$ . Gravitational effects are relevant in the context of U-tube oscillations in  $^4\text{He}$  as studied by P. W. Anderson, *Rev. Mod. Phys.* **38**, 298 (1969).
- [31] R. J. Ballagh, K. Burnett, and T. F. Scott, *Phys. Rev. Lett.* **78**, 1607 (1997).
- [32] V. M. Kenkre and D. K. Campbell, *Phys. Rev. B* **34**, 4959 (1986).
- [33] T. A. Fulton, in *Superconductor Applications: SQUIDS and Machines*, edited by B. B. Schwartz and S. Foner (Plenum, New York, 1976).
- [34] J. M. Golden and B. I. Halperin, *Phys. Rev. B* **53**, 3893 (1996).
- [35] S. V. Pereverzev, A. Loshak, S. Backhaus, J. C. Davis, and R. E. Packard, *Nature* **388**, 449 (1997).
- [36] S. Backhaus, S. V. Pereverzev, A. Loshak, J. C. Davis, and R. E. Packard, *Science* **278**, 1435 (1998).
- [37] L. N. Bulaevskii *et al.*, *JETP Lett.* **25**, 290 (1977); V. B. Geshkenbein *et al.*, *Phys. Rev. B* **36**, 25 (1987); D. A. Wollman *et al.*, *Phys. Rev. Lett.* **74**, 797 (1993).
- [38] See S. Raghavan, V. M. Kenkre, D. H. Dunlap, A. R. Bishop, and M. I. Salkola, *Phys. Rev. A* **54**, R1781 (1996), and references therein.
- [39] S. Giovanazzi, Ph.D. thesis, SISSA-ISAS, 1998, (unpublished).
- [40] V. M. Kenkre in *Singular Behavior and Nonlinear Dynamics*, edited by St. Pnevmatikos, T. Bountis, and Sp. Pnevmatikos, (World Scientific, Singapore, 1989); V. M. Kenkre, *Physica D* **68**, 153 (1993).

- [41] V. M. Kenkre and G. P. Tsironis, Phys. Rev. B **35**, 1473 (1987).
- [42] S. Raghavan, V. M. Kenkre, and A. R. Bishop, Phys. Lett. A **233**, 73 (1997).
- [43] P. F. Byrd and M. D. Friedman, *Handbook of elliptic integrals for engineers and scientists*, 2<sup>nd</sup> ed., (Springer, Berlin, 1971).; L. M. Milne-Thomson, in *Handbook of Mathematical Functions*, edited by M. Abramowitz and I. A. Stegun (Dover, New York, 1970).
- [44] G. P. Tsironis, Ph.D. thesis, University of Rochester, 1986, (unpublished).
- [45] J. D. Andersen and V. M. Kenkre, Phys. Rev. B **47**, 11134 (1993).
- [46] V. M. Kenkre and M. Kuś, Phys. Rev. B **46**, 13792 (1992).

## FIGURES

FIG. 1. The asymmetric double well trap for two Bose-Einstein condensates with  $N_{1,2}$  and  $E_{1,2}^0$ , the number of particles and the zero-point energies in the traps 1 and 2 respectively.

FIG. 2. Population imbalance  $z(t)$  as a function of dimensionless time  $2\mathcal{K}t$  (in units of  $\hbar$ ), with conditions  $\Lambda = 10, \phi(0) = 0$ , symmetric trap. The initial population imbalance  $z(0)$  takes the values: a)0.1, b)0.5, c)0.59, d)0.6, e)0.65.

FIG. 3.  $z(t)$  as a function of  $2\mathcal{K}t$  with initial conditions  $z(0) = 0.6, \phi(0) = \pi$ , symmetric trap.  $\Lambda$  takes the values: a)0.1, b)1.1, c)1.111, d)1.2, e)1.25, f)1.3.

FIG. 4. The  $\phi$ -potential  $V(\phi)$  (in arb. units) plotted against  $\phi/\pi$  for  $\Lambda = 0.2, 0.4, 0.6$ .

FIG. 5. The  $z$ -potential  $W(z)$  (in arb. units) plotted against  $z$  in a) and c) and the corresponding  $\phi$ -evolution shown in b) and d). In a),b)  $\phi(0) = 0$ , and in c),d)  $\phi(0) = \pi$ . The values of  $z(0)$  are as shown.

FIG. 6. The inverse period (scaled in units of  $2\mathcal{K}$ )  $1/\tau$  plotted against  $z(0)/z_c$  for a) $\phi(0) = 0$ , b) $\phi(0) = \pi$ . In a), the dashed line corresponds to  $\Lambda = 10$ , for which the dip occurs at  $z_c = 0.6$  and the solid line to  $\Lambda = 100$ , for which  $z_c = 0.2$ . The inset in a) shows the time-averaged population imbalance  $\langle z \rangle$  as a function of  $z(0)/z_c$ . In b),  $\Lambda = 1.111, z_c = 0.6$ .

FIG. 7. The phase-plane portrait of the dynamical variables  $z$  and  $\phi$  for  $\Lambda/\Lambda_c$  values as marked. For all trajectories,  $z(0) = 0.6$ . See text for explanation of the markings of the various trajectories.

FIG. 8. Universal curve for data-collapse with  $(\pi/(\mathcal{K}C\Lambda^2\tau))$  (in units of  $\hbar$ ) versus  $k^2(\Lambda)$  as in Eq. (B6b).



FIG. 9. Scaled inverse period  $\tau_{ac}/\tau$  plotted against  $\Lambda$  for fixed asymmetric trap parameter  $\Delta E = 1$ ,  $z(0) = 0.1$ , and  $\phi(0) = 0, \pi$  initial values, and  $1/\tau_{ac}$  as defined in Eq. (4.7). The vertical scale on the left (right) corresponds to  $\phi(0) = 0(\pi)$ . The insets show time-averaged  $\langle z \rangle$  against  $\Lambda$ , for (a),  $\phi(0) = 0$  and (b),  $\phi(0) = \pi$ .

FIG. 10. Analog of Shapiro effect: dc current  $I_{dc} = \langle \dot{z} \rangle$  versus trap asymmetry parameter scaled in applied frequency,  $\Delta E/\omega_0$ . Here  $z(0) = 0.045$ ,  $\phi(0) = \pi/2$ ,  $\Delta E_1/\omega_0 \hbar = 3.5$ , and dashed (thick solid) lines are for  $\Lambda = 0(1000)$ .

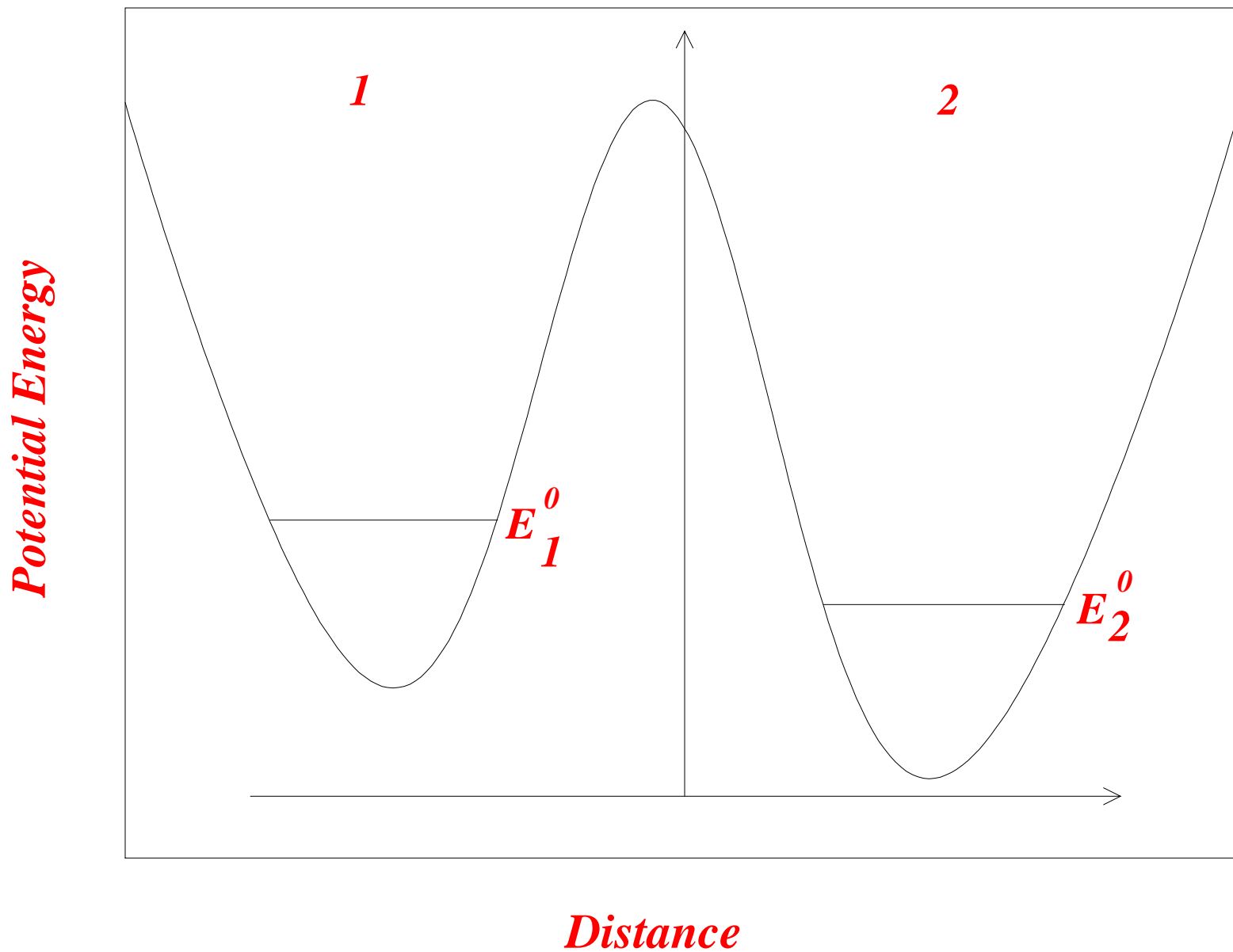
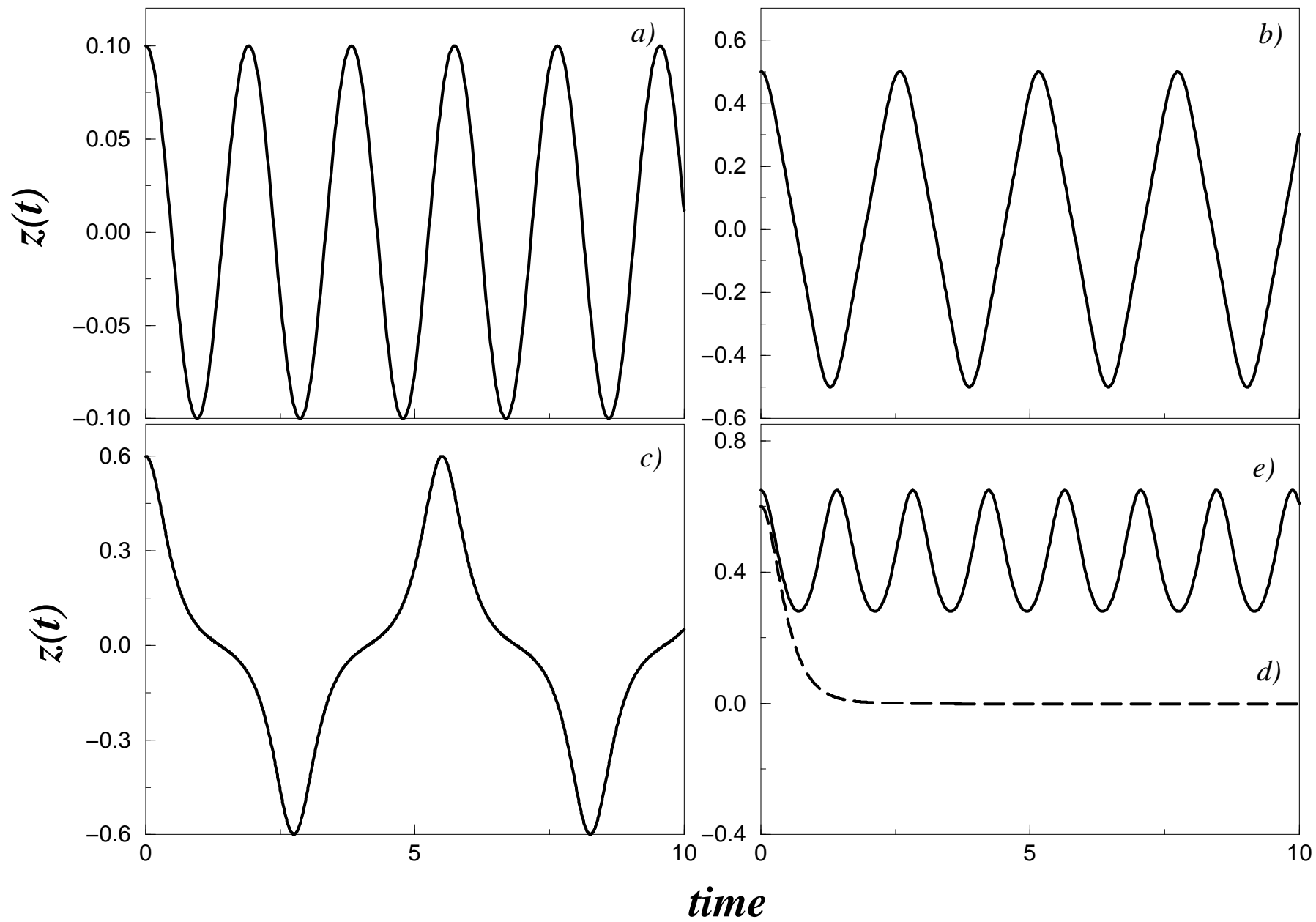
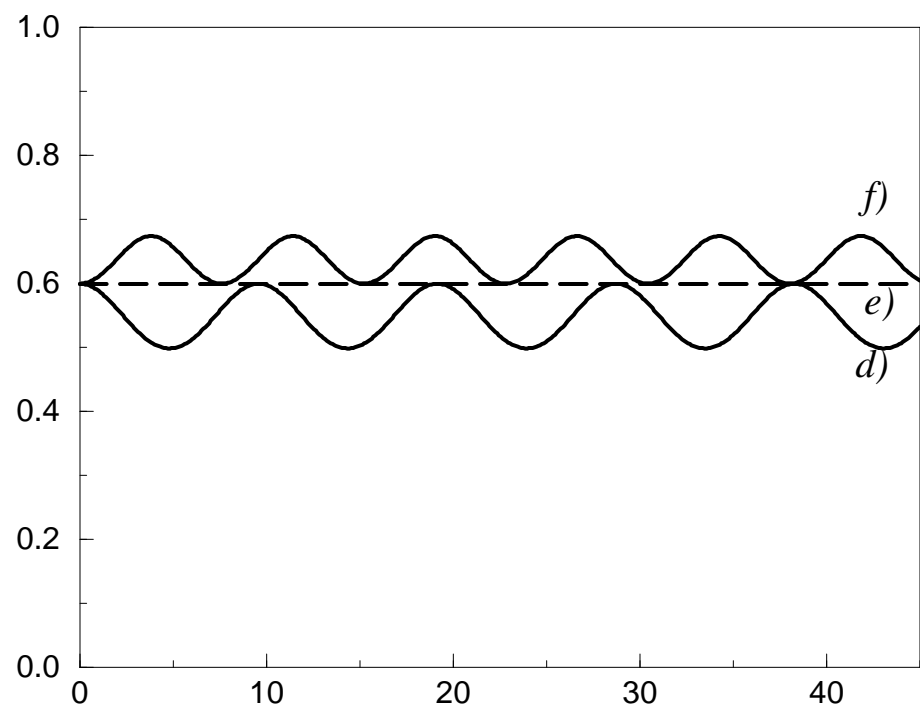
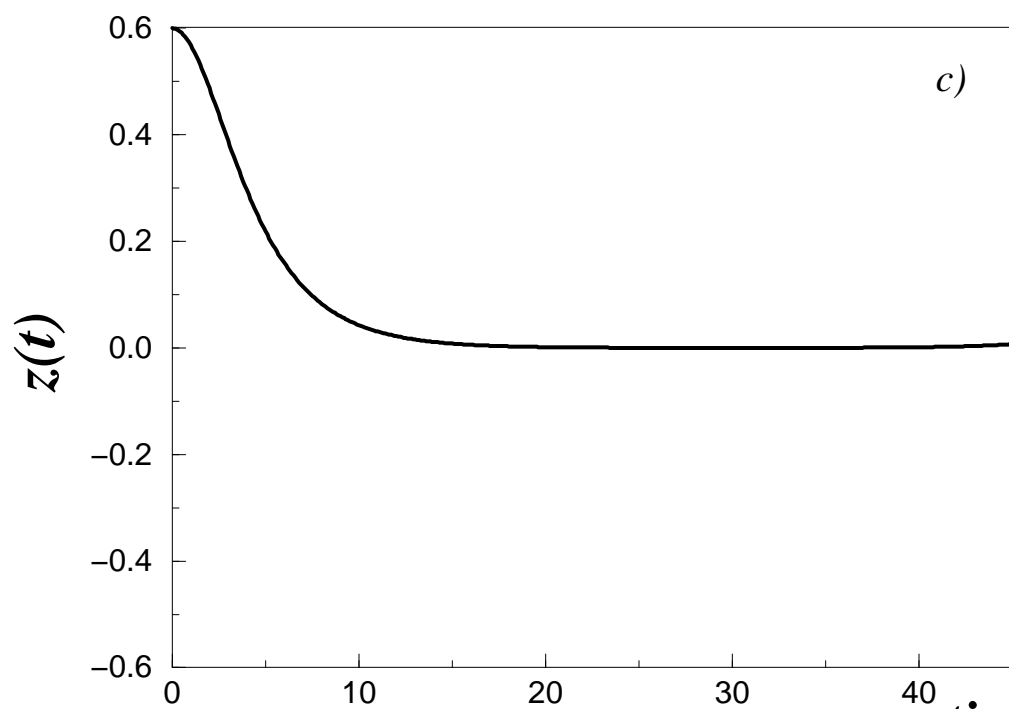
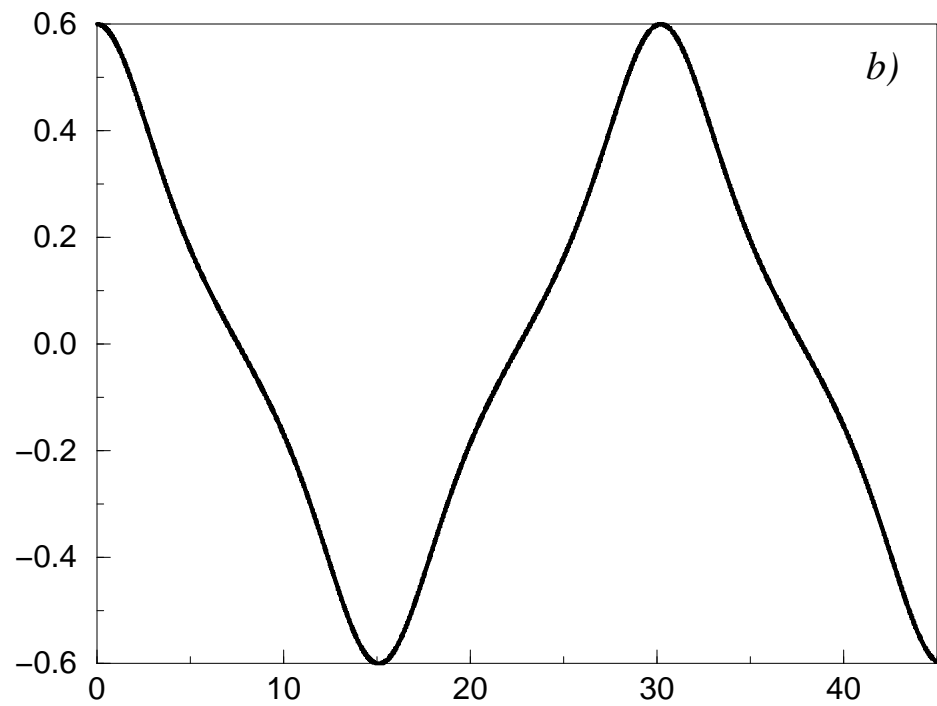
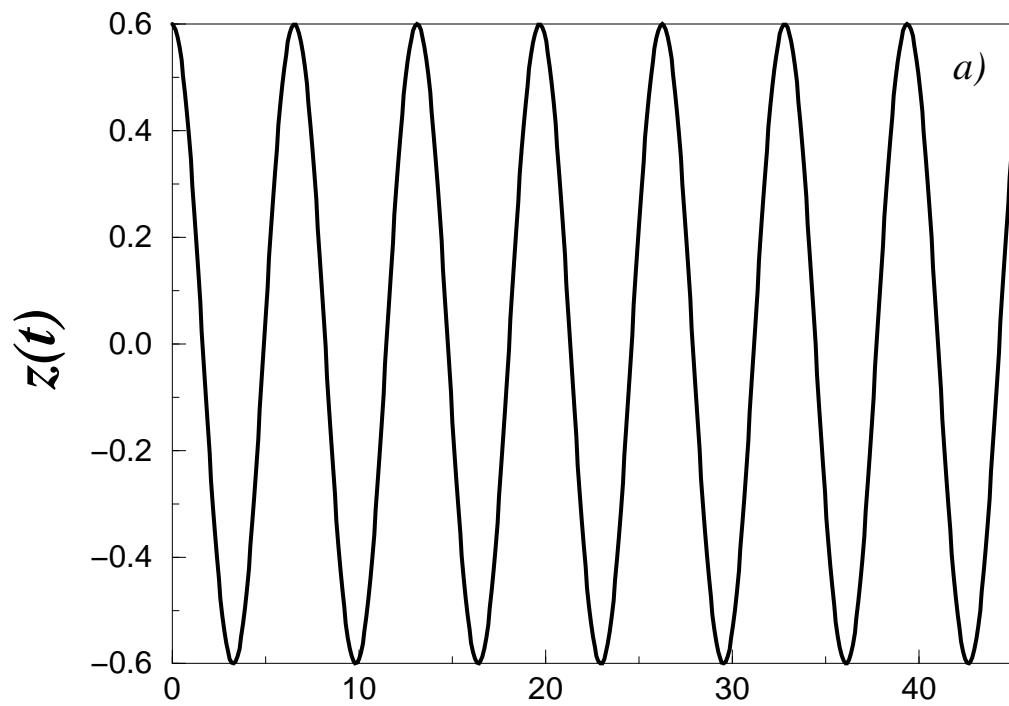
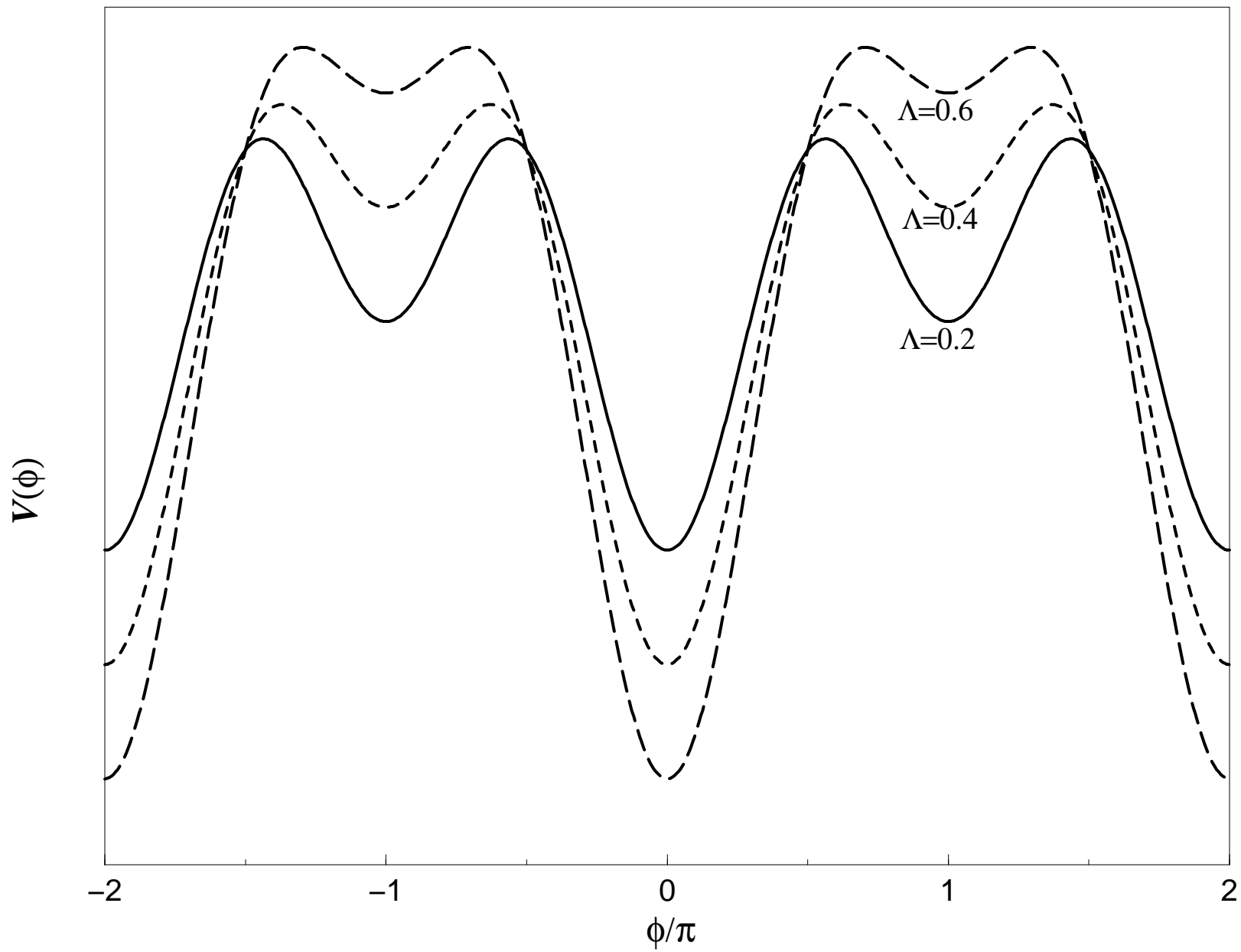


Fig.1





*time*



$\phi(0)=0, \Lambda=10$

$\phi(0)=\pi, \Lambda=2.5$

